Influence of Acid Hydrolysis Reaction Time on the Isolation of Cellulose Nanowhiskers from Oil Palm Empty Fruit Bunch Microcrystalline Cellulose

Nasrullah Razali,[a] Md. Sohrab Hossain,[b] Owolabi Abdulwahab Taiwo,[c] Mazlan Ibrahim,[d] Nur Wahidah Mohd Nadzri,[d] Nadhilah Razak,[d] Nurul Fazita Mohammad Rawi,[d] Marliana Mohd Mahadar,[e] and Mohamad Haafiz Mohamad Kassim [d]*

Cellulose nanowhiskers (CNW) were successfully isolated from oil palm empty fruit bunch microcrystalline cellulose (OPEFB-MCC) through sulfuric acid (H_2SO_4) hydrolysis with different reaction times. OPEFB-MCC was hydrolyzed with 64 wt.% H_2SO_4 at 40 °C and various reaction times (30, 60, and 90 min). Effects of the hydrolysis time on the morphologies and properties of the cellulose were evaluated by Fourier transform infrared (FTIR) spectroscopy, X-ray diffraction (XRD), thermogravimetric analysis (TGA), differential scanning calorimetry (DSC), and transmission electron microscopy (TEM). The FTIR analysis showed that the chemical compositions of all of the samples were the same and represented the cellulose I structure. Hydrolysis time had little effect on the crystallinity index of the CNW, as was revealed by the XRD. The TEM images showed that the CNW produced with different reaction times had a rod-like shape and similar diameters and lengths. The produced CNW had better thermal stabilities than the OPEFB-MCC.

Keywords: Oil palm empty fruit bunch; Cellulose nanowhiskers; Acid hydrolysis; Crystallinity index; Transmission electron microscopy

*Contact information: a: Department of Chemical Engineering, Syiah Kuala University Banda Aceh, 23111 Indonesia; b: Universiti Kuala Lumpur, Malaysian Institute of Chemical & Bioengineering Technology, 78000 Alor Gajah, Melaka, Malaysia; c: Federal Institute of Industrial Research Oshodi PMB 21023 Ikeja, Lagos, Nigeria; d: School of Industrial Technology, Universiti Sains Malaysia, Penang Malaysia; e: Faculty of Chemical and Energy Engineering, Universiti Teknologi Malaysia, 81310 Skudai, Johor Bahru, Malaysia; * Corresponding author: mhaafiz@usm.my*

INTRODUCTION

There has been an increasing demand for the isolation of biodegradable materials from lignocellulosic biomass because of its widespread applicability, sustainability, and minimization of dependence on fossil fuel. Oil palm empty fruit bunch (OPEFB) is one of the most abundant biomass materials available in palm oil producing countries. Along with the unprecedented increase in the palm oil industry in Malaysia, the generation of OPEFB is increasing every year. It is estimated that every tonne of palm oil produced from fresh fruit bunch generates 1.07 tonnes of OPEFB. Based on the 19.5 million tonnes of crude palm oil produced in Malaysia in 2015, the annual OPEFB generation from the palm oil industry is estimated to be 20.86 million tonnes. If this large quantity of generated OPEFB is not handled properly, it could pose a severe environmental pollution threat. However,

there is a growing interest in utilizing OPEFB as value-added products because of its favorable physicochemical properties (Zahrim *et al.* 2015). The most remarkable property of OPEFB is its high cellulose content, which has a variety of potential applications in the chemical, food, and composite industries (Majeed *et al.* 2013). Rosnah *et al*. (2002) reported that OPEFB contains 40% to 43% cellulose, 22% to 25% hemicellulose, and 19% to 21% lignin. Cellulose is a naturally occurring polymer in plants and is comprised of glucose units joined together by β-1,4 glycosidic bonds. The linear cellulose chains are bundled together as microfibrils, and these microfibrils are composed of amorphous and crystalline regions. Amorphous regions exhibit weaker internal bonds, while crystalline regions exhibit strong internal bonds (Ramli *et al.* 2015).

Cellulose is the most abundant and naturally occurring polymer. It has been widely used as reinforcement material in biopolymers (Fatah *et al*. 2014). Cellulosic fiber consists of bundles of several cellulose nanofibers. The crystalline part of these cellulose nanofibers, once it has been separated from the biomass, is known by such terms as cellulose nanowhiskers (CNW) and cellulose nanocrystals (CNC). CNW are nano-sized rod-shaped crystals that can be isolated from cellulosic materials (microcrystalline cellulose) by acid hydrolysis. CNW are a type of filamentary crystal (whisker) with a cross sectional diameter that ranges from 1 to 100 nm and a length to diameter ratio (L/d) that is greater than 100. CNW can be isolated from various lignocellulosic materials with several preparation techniques. Sulfuric acid hydrolysis of the amorphous region completely hydrolyzes the cellulose and yields highly crystalline CNW, which can potentially be applied as an effective reinforcement in polymeric composite materials (Haafiz *et al.* 2013). CNW have received increasing attention because of the extraordinary mechanical properties, such as a high Young's modulus and tensile strength (Carpenter *et al.* 2015). Cellulose nanoparticles have also been synthesized in spherical forms and rod-like highly crystalline nanocrystals by acid hydrolysis of cellulosic fibers. Microfibrillated cellulose can be obtained from the disintegration of cellulose fibers under high shearing and impact forces (Teixeira *et al.* 2009).

Acid hydrolysis of cellulose is a well-known chemical process that uses a strong acid, such as sulfuric or hydrochloric acid, to remove the amorphous region. Studies have been conducted on the isolation of CNW from the microcrystalline cellulose (MCC) of various natural fibers using acid hydrolysis. For instance, Haafiz *et al.* (2013) successfully isolated CNW from the MCC of OPEFB. It was reported that the acid hydrolysis process resulted in the transverse cleavage of nanofibril bundles, which broke down the hierarchical structure into crystalline nanofibers (CNF) or CNC (Ng *et al.* 2015). The morphology of CNW obtained using acid hydrolysis is influenced by several factors, including the acid-to-pulp ratio, reaction time, temperature, and cellulose source (Pandey *et al.* 2013). The reaction time is one of the most crucial factors of the acid hydrolysis process because a sufficient reaction time is required to break down the hierarchical structure of the fiber into a nanocrystalline structure. Unfortunately, very few studies have considered the effect from the acid hydrolysis reaction time on the mechanical, thermal, and morphological properties of the CNW.

The present study was conducted to determine the characteristic properties of the CNW produced at various reaction times. The influence of the acid hydrolysis reaction time on the isolation of the CNW was analyzed using Fourier transform infrared (FTIR)

spectroscopy. The crystallinity index was studied using X-ray diffraction (XRD), while the thermal characterization was carried out using thermogravimetric analysis (TGA) and differential scanning calorimetry (DSC). The morphological transformation of the samples was monitored with transmission electron microscopy (TEM).

EXPERIMENTAL

Materials

OPEFB was used as the raw material for the isolation of oil palm empty fruit bunch microcrystalline cellulose (OPEFB-MCC) and was obtained from United Oil Palm Industries Sdn. Bhd. (Nibong Tebal, Malaysia). The OPEFB-MCC was obtained using the technique reported by Haafiz *et al*. (2013). The chemicals used were hydrochloric acid (HCl) (37%), magnesium sulphate ($MgSO_4.7H_2O$; 99%), sodium hydroxide (NaOH), sulfuric acid (H_2SO_4, 98%), and hydrogen peroxide (H_2O_2, 30%). All of the chemicals were of analytical grade, purchased from Sigma Aldrich and used as received.

Production of the Microcrystalline Cellulose (MCC)

The MCC was isolated from totally chlorine free (TCF) OPEFB-pulp using the technique described by Haafiz *et al*. (2013) and Chuayjuljit *et al.* (2009), which was based on the original procedures reported by Battista (1950). The TCF OPEFB-pulp was hydrolyzed with 2.5 N HCl with a solid to liquid ratio of 1:20 (TCF OPEFB-pulp to 2.5 N HCl) at 105 °C for 20 min under condensation. The product was thoroughly washed with distilled water and dried at 40 °C for 24 h. The MCC produced was snowy-white in appearance and labelled as OPEFB-MCC.

Preparation of the Cellulose Nanowhiskers (CNW) from OPEFB-MCC

The isolation of CNW from the OPEFB-MCC was done according to the method reported by Haafiz *et al*. (2013) with some modifications. Five grams of OPEFB-MCC were hydrolyzed in a 64% H_2SO_4 solution at a ratio of 8.75 mL/g and 40 °C. The reaction times used for the acid hydrolysis were 30, 60, and 90 min with strong agitation, and the isolated CNW were labelled CNW-30, CNW-60, and CNW-90, respectively. The hydrolysis reaction was quenched by adding a 4- to 5-fold amount of cold distilled water, which was followed by centrifugation with a Kubota 5100 centrifuge (Tokyo, Japan) at 20,000 rpm for 20 min. The sediment was collected and dialyzed using dialysis tubing cellulose membrane (Sigma Aldrich) with a molecular weight cut off at 12 to 14 kDa, and then it was washed again with distilled water until a neutral pH was obtained. After dialysis, the suspension was sonicated for 30 min to disperse the nanofibers. Sonication was done in a Branson 2510 water bath (Gaithersburg, MD, USA) to avoid overheating. The resultant aqueous suspension of CNW was centrifuged at 20,000 rpm for 20 min, which was then freeze-dried for characterization. The CNW yield was determined by following the method reported by Davoudpour *et al*. (2015) and Eq. 1:

$$\text{Yield}(\%) = \left(1 - \frac{\text{weight of dried sediment (g)}}{\text{weight of diluted sample (g)} \times \%\text{SC}}\right) \times 100 \quad (1)$$

Characterization of the CNW Samples

Fourier transform infrared (FTIR) spectroscopy

The chemical structure of the prepared CNW after acid hydrolysis was studied using an Avatar 360 FTIR spectrometer (Madison, United States). The samples were pelletized, and the FTIR spectra of the OPEFB-MCC, CNW-30, CNW-60, and CNW-90 were obtained using the KBr method with a ratio of 1:100. The FTIR spectra of the coated pellets were recorded within the wavenumber range of 600 to 4000 cm^{-1}. The major transmittance peaks at particular wavenumbers were measured by using the Origin Pro 2016 software (Originlab Corporation, Wellesley Hills, MA, USA).

X-ray diffraction (XRD)

The crystallinity study of the CNW samples was performed using a BRUKER AXS-D8 ADVANCE (Karlsruhe, Germany). The XRD patterns were scanned at intervals of 0.0034° over a 2θ range of 10° to 50° and using monochromatic Cu Kα radiation as an X-ray source with a wavelength (λ) of 0.154021 nm at 40 kV and 40 mA. The crystallinity index of the cellulose (%) was calculated based on the Segal *et al*. (1959) method and using Eq. 2:

$$CI(\%) = \frac{I_{cry} - I_{ams}}{I_{cry}} \times 100 \quad (2)$$

where *CI* is the crystallinity index (%), I_{cry} is the maximum intensity at a 2θ of 22° to 24°, and I_{ams} is the intensity of the amorphous material at an angle of approximately 18° in the valley between the peaks.

Thermogravimetric analysis (TGA)

The thermal stability of the CNW samples was characterized by using a thermogravimetric analyzer (Mettler-Toledo TGA/DSC, Schwerzenbach, Switzerland). Ten milligrams of a sample were put into the sample holder and heated at a rate of 10 °C/min in a nitrogen flux atmosphere from room temperature to 800 °C. The thermogram recorded the percentage of weight loss *versus* temperature. The mass change of the sample was recorded continuously over the entire temperature and time ranges.

Differential scanning calorimetry (DSC) analysis

The thermal behavior of the CNW was monitored using DSC. The analysis was conducted from 30 to 400 °C with intermittent heating and cooling, which was done twice with the purpose of determining the phase changes that occurred during analysis. In this analysis, heating was first conducted from 30 to 100 °C, and the sample was then cooled back to room temperature. The moisture in the sample was removed and the heating process occurred again, this time from 30 to 400 °C with a 10 °C/min heating rate. The time it took to heat each sample was almost 150 min.

Transmission electron microscopy (TEM)

The dimensions of the prepared CNW samples were obtained with TEM on a Philips CM12 image analyzer (Version 3.2, Amsterdam, Netherlands). Drops of the 0.001 wt.% CNW suspension were deposited on a glow-discharged carbon-coated 200-mesh

copper grid and dried for 5 min at ambient temperature. The samples were negatively stained with 2% phosphotungstic acid prior to analysis.

RESULTS AND DISCUSSION

Preparation of the CNW

The production of the CNW from the OPEFB-MCC was conducted using 64% H_2SO_4 solution with a ratio of 8.75 mL/g at 40 °C for 30 to 90 min. It was observed that the CNW yield decreased as the acid hydrolysis reaction time increased. The CNW yields were found to be 87%, 81%, and 74% for CNW-30, CNW-60, and CNW-90, respectively.

It is well known that acid hydrolysis is the most widely utilized method in the production of CNF or CNW from various lignocellulosic fiber because of its effectiveness and possibility of lowering the energy consumption (Han *et al*. 2014; Lani *et al*. 2014). Generally, the acid hydrolysis process breaks the β-1,4 glycosidic bonds in the cellulosic fiber during the production of cellulose. H_2SO_4 is reported to be the most effective agent for acid hydrolysis.

Numerous studies have been conducted on the production of CNW from various lignocellulosic fiber using 50% to 72% H_2SO_4 solution with a 1-h reaction time (Han *et al*. 2014; Lani *et al*. 2014; Rahimi Kord Sofla *et al*. 2016). However, the degree of cellulose structure breakage highly depends on the hydrolytic reaction when subject to an acid treatment (Fatah *et al*. 2014). Thus, the thermal properties and morphological structure of isolated CNW can vary with the acid hydrolysis reaction time.

FTIR Analysis

The FTIR spectra of the CNW prepared at different reaction times showed bands that were in the functional group region, 4000 to 1300 cm^{-1}, and the fingerprint region, 1300 to 400 cm^{-1}, which are used when comparing the spectra of different products. The FTIR spectra of the OPEFB-MCC and CNW samples are shown in Fig. 1. Table 1 summarizes the vibrational assignments of the bands in the OPEFB-MCC and CNW spectra. The absorption bands near 3400, 2900, 1430, 1370, and 890 cm^{-1} were found in all of the spectra, and were associated with native cellulose I (Tang *et al.* 2013). The broad band observed in all of the samples in the region of 3300 to 3400 cm^{-1} resulted from the stretching vibrations of hydroxyl groups (Abdul Khalil *et al.* 2001). The absorption band at 2900 cm^{-1} was related to CH_2 groups in the cellulose (Jonoobi *et al.* 2011; Rosa *et al.* 2012). The band at 1640 cm^{-1} was assigned to C=C stretching of aromatic rings in lignin, while the peak that appeared at 1240 cm^{-1} was determined to be C-O-C stretching of aryl-alkyl ether linkages in lignin (Yang and Ye 2012).

The FTIR spectra showed that the chemical swelling and acid hydrolysis reaction performed to obtain CNW from the OPEFB-MCC did not affect the chemical structure of the cellulosic fragments. This implied that the chemical groups of the resulting materials were stable and no strong chemical reactions occurred (Chen and Yada 2011). The absence of characteristic bands between 1600 and 1740 cm^{-1} revealed that the isolated MCC and CNW were free of impurities (Rahimi Kord Sofla *et al*. 2016).

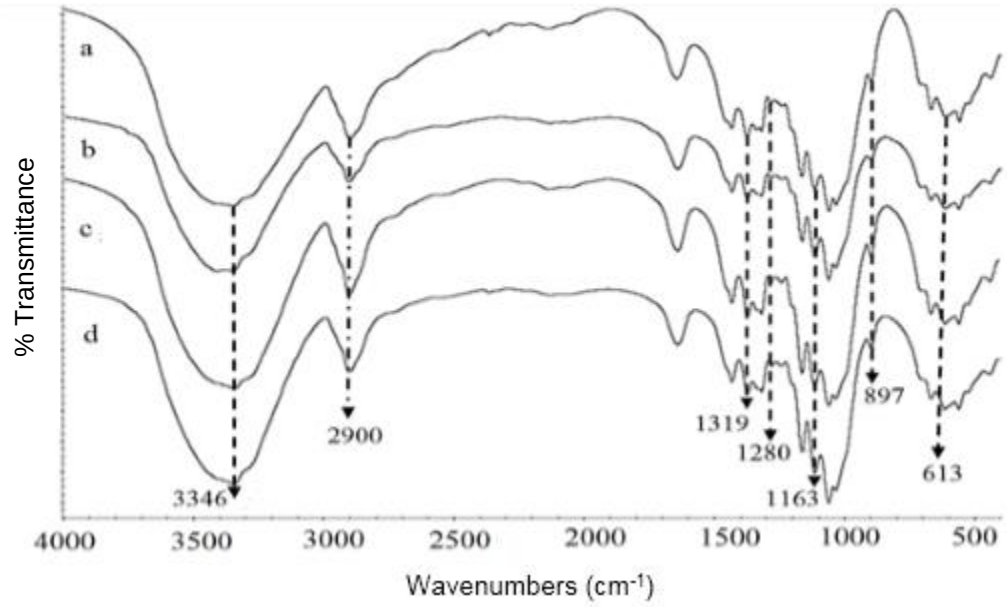

Fig. 1. FTIR spectra of the (a) OPEFB-MCC, (b) CNW-30, (c) CNW-60, and (d) CNW-90

Table 1. Peak Frequency for the OPEFB-MCC, CNW-30, CNW-60, and CNW-90

Band	OPEFB-MCC (cm^{-1})	CNW-30 (cm^{-1})	CNW-60 (cm^{-1})	CNW-90 (cm^{-1})
O-H groups	3346	3413	3345	3346
CH_2 groups	2899	2901	2900	2900
Nitriles/Carbenes	2361	-	-	2362
C=O stretching	1642	1640	1641	1640
CH_2 bending	1432	1430	1430	1430
C-H asymmetric stretching	1375	1373	1372	1372
C-O-C stretching	1164	1163	1164	1163
C-H	896	898	897	897

XRD Analysis

The degree of crystallinity is the ratio of crystalline areas to amorphous areas in the cellulose. XRD patterns of natural lignocellulosic fibers are known to display a typical cellulose type I crystal lattice with main diffraction signals at 2θ values of 15°, 16°, 22.5°, and 34° (de Moura *et al.* 2012). An XRD analysis was performed on the OPEFB-MCC and CNW to investigate the effects of the hydrolysis time on the crystalline structure. Figure 2 shows the peaks obtained for each sample. The characteristic XRD pattern for cellulose I was seen irrespective of the treatment conditions.

However, as can be seen in Table 2, the crystallinity of the CNW decreased as the reaction time increased. This might have been because of the presence of sulphate groups, which were generated from cellulose chain esterification after the acid hydrolysis. A decrease in crystallinity after acid hydrolysis was observed by Tang *et al*. (2013) in a microstructural study of CNC from pure wood pulp filter paper. Additionally, according to

Tang *et al*. (2013), this phenomenon was probably because the surface amorphous ratio of the CNW was high. As a result of the high specific surface area, differences in the thermal degradation behavior were seen. This meant that the surface amorphous ratio of CNW-60 was higher compared with the other CNW samples. CNW-30 exhibited the highest crystallinity (77.19%), followed by CNW-90 (76.81%) and CNW-60 (75.89%). For the 30 min hydrolysis time, the crystallinity was higher than that of the non-hydrolyzed fiber, which was possibly because the sulfuric acid could penetrate into the amorphous region of the cellulose, causing hydrolytic cleavage of glycosidic bonds and releasing individual crystallites (Li *et al.* 2009).

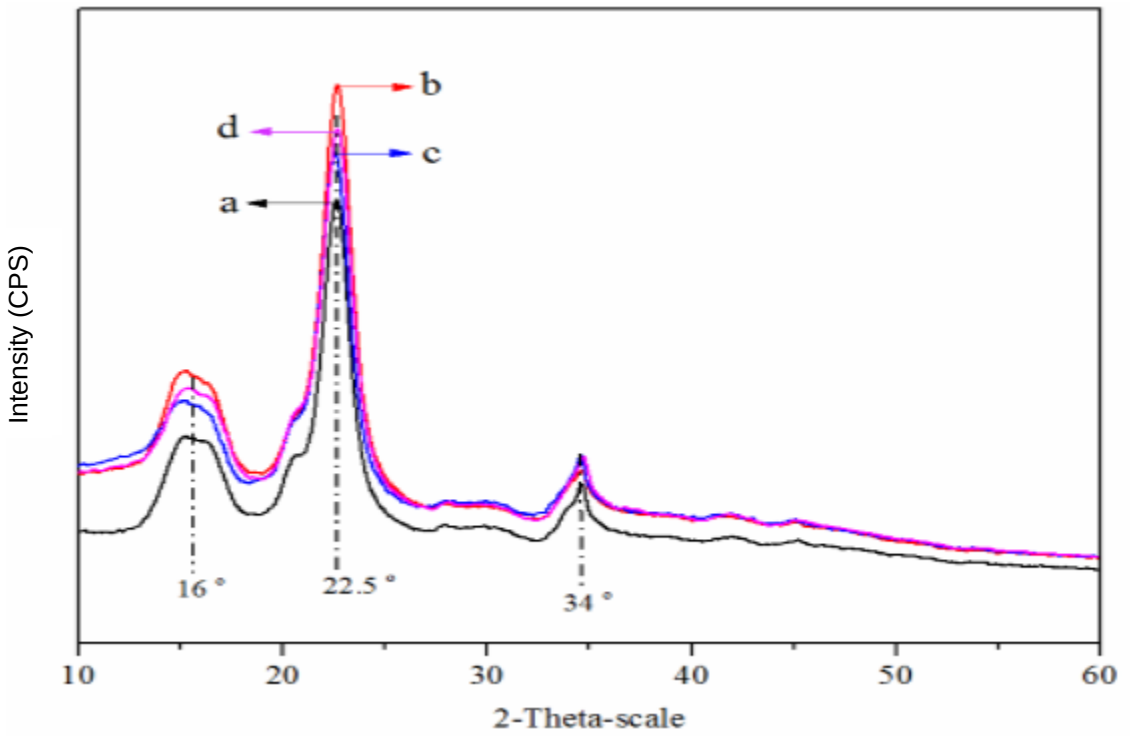

Fig. 2. XRD patterns of the (a) OPEFB-MCC, (b) CNW-30, (c) CNW-60, and (d) CNW-90

Generally, acid cannot rapidly penetrate the crystalline regions because those regions are resistant to acid hydrolysis. During cellulose hydrolysis, the amorphous regions are attacked by acid. Despite the drastic conditions of hydrolysis, the amorphous and crystalline regions may only be partially destroyed because of the corrosion caused by the high concentration of sulfuric acid (Chen *et al*. 2009). This was the reason why the crystallinity of the nanofibers tended to decrease as the hydrolysis time increased, which indicated that 30 min was enough time to remove the amorphous regions in the OPEFB cellulose fiber. A study reported that the sulphate ions in the acid hydrolysis process penetrated the hydrolytic cleavage of glyosidic bonds and released the individual crystallites (Nishiyama *et al*. 2002). Their results were supported by the FTIR analysis results.

Table 2. Crystallinity of the OPEFB-MCC, CNW-30, CNW-60, and CNW-90

Sample	Crystallinity (%)
OPEFB-MCC	80.81
CNW-30	77.19
CNW-60	75.89
CNW-90	76.81

TGA

The TGA and differential thermogravimetric (DTG) curves of the OPEFB-MCC and CNW samples are shown in Figs. 3 and 4, respectively. The thermal stability of the samples was characterized by the temperature at 10% (T_{10}) and 50% (T_{50}) of the sample weight loss. There was an initial weight loss detected from 30 to 200 °C for all of the samples because of the evaporation of water in the cellulose microfibers and nanofibers. CNW-30, CNW-60, and CNW-90 began to decompose at 170, 230, and 201 °C, respectively, whereas the OPEFB-MCC was stable until a much higher temperature, up to 270 °C, because a higher cellulose crystallinity can delay the degradation process and improve the thermal stability (Liu *et al.* 2010).

The thermal degradation data (T_{10}, T_{50}, and temperature of the maximum weight loss (T_{max})) and residual weight at 700 °C are listed in Table 3. The T_{10} showed that CNW-60 degraded at a higher temperature (236 °C) compared with the OPEFB-MCC (54 °C), CNW-30 (193 °C), and CNW-90 (225 °C). A slight difference was observed for T_{50}, where it was CNW-30 that had a higher degradation temperature (346 °C) compared with the other samples.

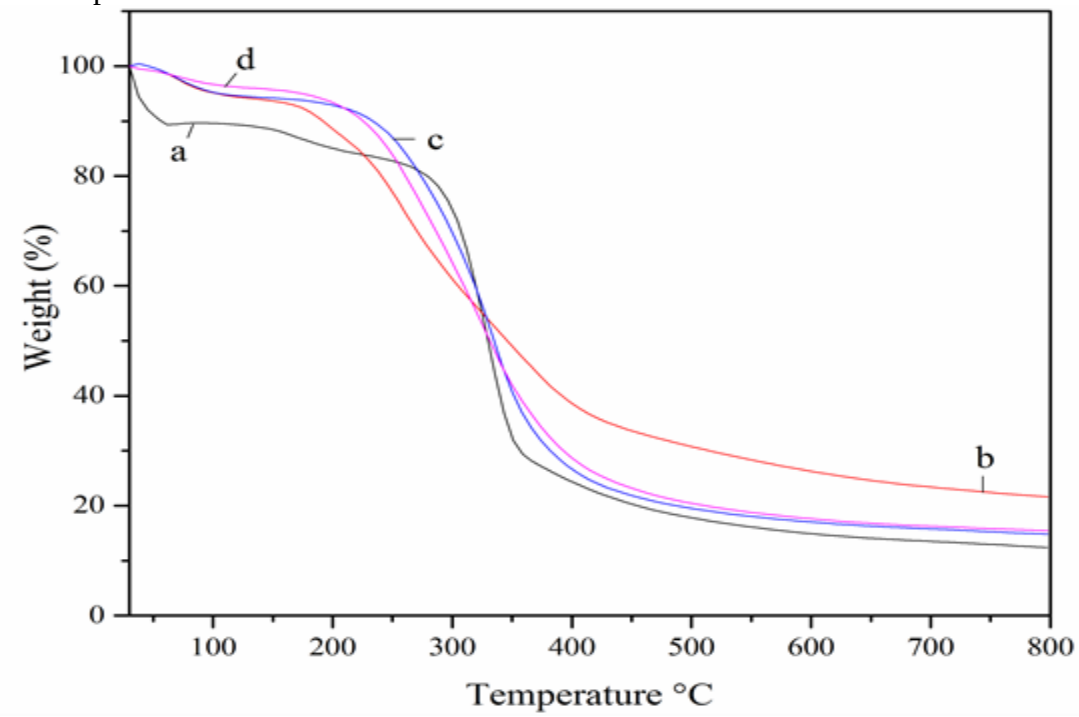

Fig. 3. TGA curves of the (a) OPEFB-MCC, (b) CNW-30, (c) CNW-60, and (d) CNW-90

Figure 4 clearly reveals that the acid hydrolysis treatment changed the thermal stability of the CNW, as all of the CNW samples had higher degradation temperatures (T_{10} and T_{50}) compared with the OPEFB-MCC. This demonstrated that the CNW had better thermal stability compared with the OPEFB-MCC. CNW-60 presented higher degradation temperatures (T_{max} and T_{10}) compared with the OPEFB-MCC and other CNW samples, which indicated that CNW-60 had the best thermal stability. The higher decomposition temperature obtained for CNW-60 was attributed to the higher crystallinity of the cellulose material (Rosa *et al.* 2012). Also, the rearrangement and reorientation of the crystals in the cellulose increased the onset degradation temperature (Mandal and Chakrabarty 2011). However, CNW-30 showed a different degradation behavior than OPEFB-MCC, CNW-60, and CNW-90. As can be seen in the DTG curves, a lower degradation at T_{max} was recorded and two shoulders appeared before and after degradation for CNW-30.

The difference in the thermal degradation behavior of the CNW arose from the differences in the outer surface structure of the nano-crystalline particles, including the presence of sulphate groups (Wang *et al.* 2007). According to Oksman *et al.* (2006), during the acid hydrolysis of the OPEFB-MCC with H_2SO_4, sulphate groups were introduced to the surface of the CNW. These sulphate groups probably affected the thermal stability of the CNW because of the dehydration reaction. It is also believed that cellulose hydrolysis not only dissolved the amorphous regions, but some crystalline regions as well, which made the cellulose more susceptible to degradation at elevated temperatures (Bras *et al.* 2010; Mandal and Chakrabarty 2011).

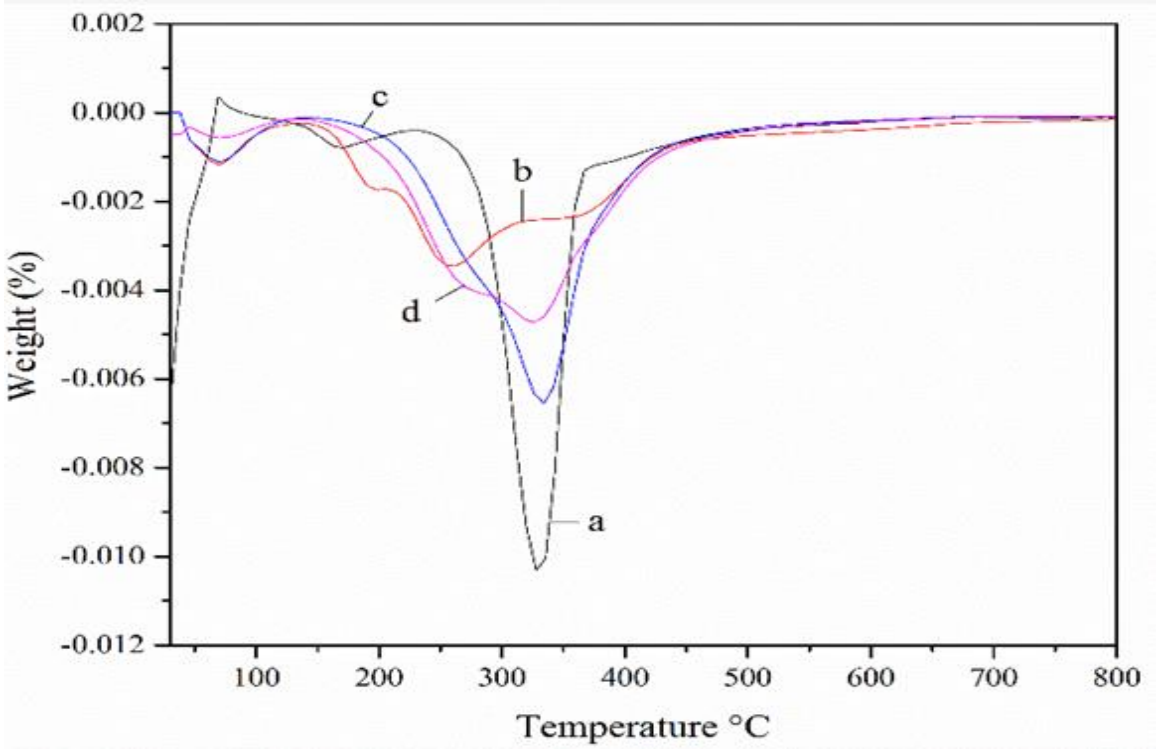

Fig. 4. DTG curves of the (a) OPEFB-MCC, (b) CNW-30, (c) CNW-60, and (d) CNW-90

CNW-30 showed higher weight residues at 700 °C compared with CNW-60 and CNW-90. This may have been because of the presence of sulphate groups, which acted as

a flame retardant and ostensibly served as a protective barrier for the attached polymeric chains against the burning surface (Li *et al.* 2009). Additionally, the dialysis process for CNW-30 was ineffective because the dialysis time was shorter, which meant a larger amount of sulphate remained on the cellulose. Rahimi Kord Sofla *et al*. (2016) found an onset degradation temperature of 204 °C for cellulose nanocystalline fiber during acid hydrolysis treatment using a 64% H_2SO_4 solution at 45 °C for 60 min. Taking into consideration the above results, it was concluded that the CNW from the OPEFB-MCC produced by acid hydrolysis at three different reaction times had better thermal stability than the OPEFB-MCC and is suitable for use as reinforcements in the production of green bio-composites.

Table 3. Thermal Degradation of the Microcrystalline Cellulose and Cellulose Nanowhiskers

Sample	T_{10} (°C)	T_{50} (°C)	T_{max} (°C)	Residual Weight (%)
OPEFB-MCC	54	331	328	13.40
CNW-30	193	346	257	23.65
CNW-60	236	339	333	15.96
CNW-90	225	333	327	16.82

DSC Analysis

DSC was used to determine the thermal behavior of the OPEFB-MCC and CNW. DSC curves of the OPEFB-MCC, CNW-30, CNW-60, and CNW-90 are shown in Fig. 5.

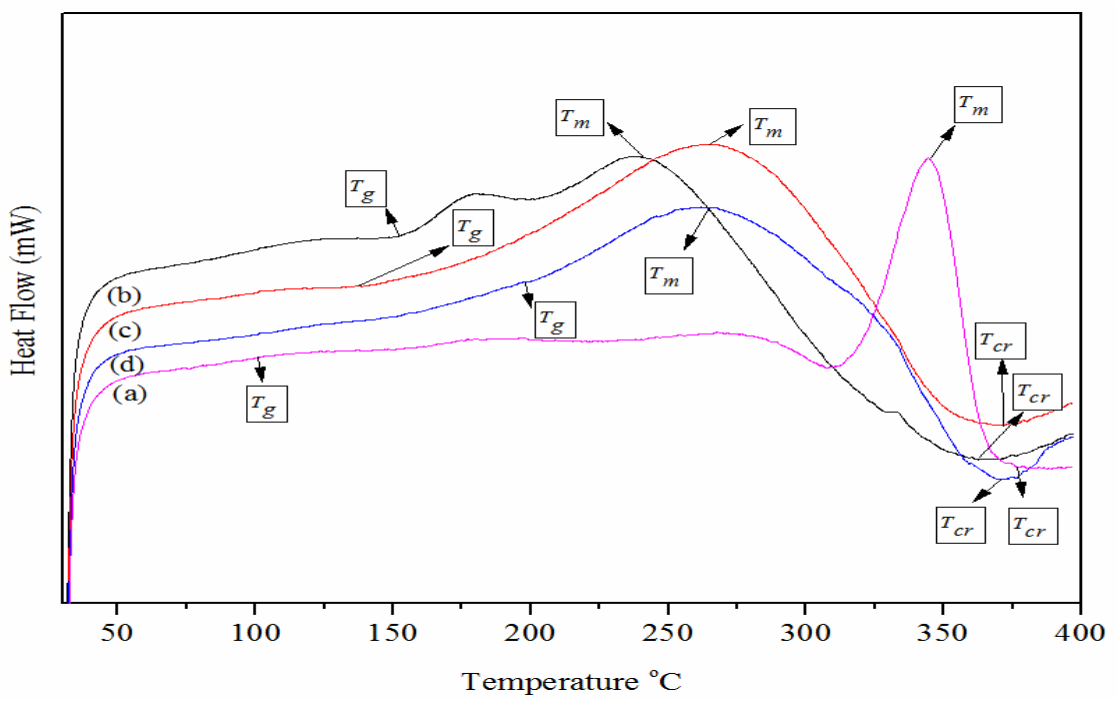

Fig. 5. DSC curves of the (a) OPEFB-MCC, (b) CNW-30, (c) CNW-60, and (d) CNW-90

Table 4 shows the values obtained for the T_g, T_m, and T_{cr}, which are the glass transition temperature, melting point, and crystallization temperature, respectively. The OPEFB-MCC curve showed an initial endothermic peak at 101 °C. This peak corresponded to the T_g of the OPEFB-MCC. The next peak at 345 °C was the T_m, and the exothermic peak at 370 °C was the T_{cr} of the OPEFB-MCC.

The curves of CNW-60 and CNW-90 had similar patterns and decomposed at lower temperatures. The curves for CNW-60 and CNW-90 had higher T_m values, 260 and 265 °C, and the T_{cr} values were 360 and 365 °C, respectively. However, their T_g values were inversely proportional, as the T_g of CNW-30 was higher than that of CNW-60, which were 150 and 140 °C, respectively.

This might have been because CNW-60 had a lower crystallinity, as revealed by the XRD analysis, and hence there were fewer hydrogen bonds between the cellulose of CNW-60 and heat changes took place. CNW-30 showed heat changes took place at 100 °C because the hydrogen bonding was lower, and an endothermic transition occurred at 240 °C, which was the T_m. The T_{cr} for all of the samples ranged between 360 to 370 °C, including for CNW-30, which was 360 °C.

Table 4. Thermal Properties of the OPEFB-MCC, CNW-30, CNW-60, and CNW-90

Samples	T_g (°C)	T_m (°C)	T_{cr} (°C)
MCC	100	345	370
CNW-30	150	240	360
CNW-60	140	260	365
CNW-90	195	260	370

TEM Analysis

The CNW obtained from the OPEFB-MCC at different acid hydrolysis times were analysed by TEM. The TEM images of the CNW are displayed in Fig. 6, and the average length is summarized in Table 5. As shown in Fig. 6, a rod-like structure for the CNW was observed after hydrolysis. This revealed that different hydrolysis reaction times were able to produce CNW with different average lengths, where the longest reaction time had the shortest average length.

Agglomeration of the CNW was observed for all of the samples. This phenomenon could have been because of the short ultrasonication treatment. According to Oksman *et al.* (2006), ultrasonic treatment can be used to separate the swollen MCC into CNW. Also, according to Liu *et al.* (2010), it is possible that this agglomeration may have been because of the surface ionic charge (esterification) caused by the strong acid treatment. Therefore, these types of CNW tend to stack into special micro-sized particles because of surface electrostatic attraction (Liu *et al.* 2010).

It is interesting to note that the single needle-like structure of the CNW was still observed despite the agglomeration, which confirmed that the OPEFB-MCC was successfully isolated.

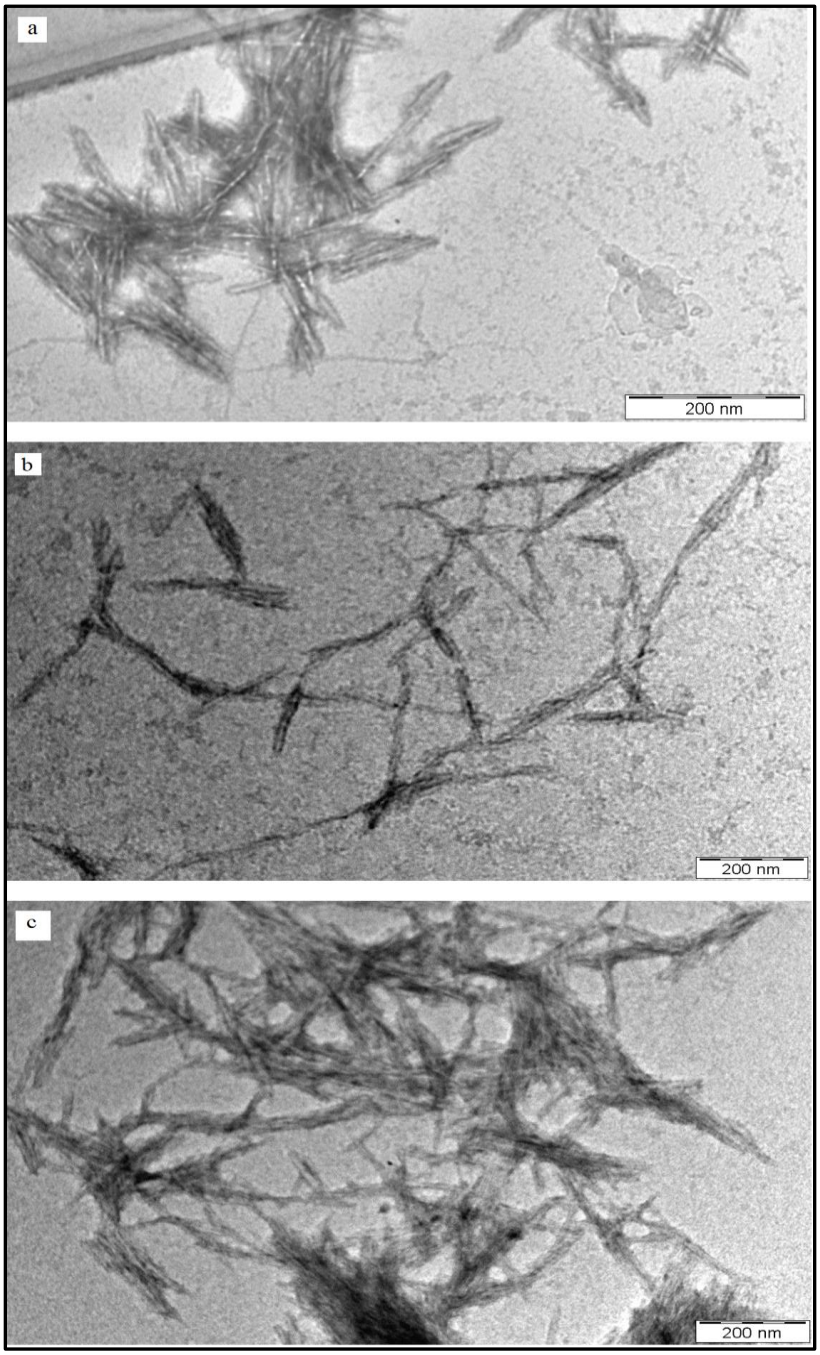

Fig. 6. TEM images of (a) CNW-30, (b) CNW-60, and (c) CNW-90

Table 5. Effect of the Hydrolysis Time on the Cellulose Nanowhiskers Structural Properties

Sample	Reaction Time (min)	Average Length (nm)	Diameter (nm)
CNW-30	30	146	6.3
CNW-60	60	132	6.0
CNW-90	90	110	5.4

CONCLUSIONS

1. CNW was successfully isolated from the OPEFB-MCC by sulfuric acid hydrolysis with three different reaction times. The experimental results showed that the average length of the CNW ranged from 110 to 150 nm and the diameter ranged from 5.4 to 6.5 nm.
2. The XRD patterns and FTIR spectra for the OPEFB-MCC, CNW-30, CNW-60, and CNW-90 showed that the characteristics of native cellulose I remained intact despite the different treatment conditions.
3. CNW-60 had the highest thermal degradation stability with the lowest amount of residual char and lowest T_g after acid hydrolysis.
4. A reaction time of 60 min was the best condition to isolate CNW from the OPEFB-MCC by the sulfuric acid hydrolysis technique.

ACKNOWLEDGMENTS

The authors would like to thank the Ministry of Higher Education for the Fundamental Research Grant Scheme (FRGS) (203/PTEKIND/6711500) and Universiti Sains Malaysia (USM) Short Term Research Grant (304/PTEKIND/6313194) for the financial support.

REFERENCES CITED

Abdul Khalil, H. P. S., Ismail, H., Ahmad, M. N., Ariffin, A., and Hassan, K. (2001). "The effect of various anhydride modifications on mechanical properties and water absorption of oil palm empty fruit bunches reinforced polyester composites," *Polym. Int.* 50(4), 395-402. DOI: 10.1002/pi.642

Battista, O. A. (1950). "Hydrolysis and crystallization of cellulose," *Ind. Eng. Chem.* 42(3), 502-507. DOI: 10.1021/ie50483a029

Bras, J., Hassan, M. L., Bruzesse, C., Hassan, E. A., El-Wakil, N. A., and Dufresne, A. (2010). "Mechanical, barrier, and biodegradability properties of bagasse cellulose whiskers reinforced natural rubber nanocomposites," *Ind. Crop. Prod.* 32(3), 627-633. DOI: 10.1016/j.indcrop.2010.07.018

Carpenter, A. W., de Lannoy, C.-F., and Wiesner, M. R. (2015). "Cellulose nanomaterials in water treatment technologies," *Environ. Sci. Technol.* 49(9), 5277-5287. DOI: 10.1021/es506351r

Chen, H., and Yada, R. (2011). "Nanotechnologies in agriculture: New tools for sustainable development," *Trends Food Sci. Tech.* 22(11), 585-594. DOI: 10.1016/j.tifs.2011.09.004

Chen, Y., Liu, C., Chang, P. R., Cao, X., and Anderson, D. P. (2009). "Bionanocomposites based on pea starch and cellulose nanowhiskers hydrolyzed from pea hull fibre: Effect of hydrolysis time," *Carbohyd. Polym.* 76(4), 607-615. DOI: 10.1016/j.carbpol.2008.11.030

Chuayjuljit, S., Su-uthai, S., and Charuchinda, S. (2009). "Poly (vinyl chloride) film filled with microcrystalline cellulose prepared from cotton fabric waste: Properties and biodegradability study," *Waste Manage. Res.* 28(2), 109-117. DOI: 10.1177/073242X09339324

Davoudpour, Y., Hossain, S., Abdul Khalil, H. P. S., Haafiz, M. K. M., Ishak, Z. A. M., Hassan, A., and Sarker, Z. I. (2015). "Optimization of high pressure homogenization parameters for the isolation of cellulosic nanofibers using response surface methodology," *Ind. Crop. Prod.* 74, 381-387. DOI: 10.1016/j.indcrop.2015.05.029

de Moura, M. R., Mattoso, L. H., and Zucolotto, V. (2012). "Development of cellulose-based bactericidal nanocomposites containing silver nanoparticles and their use as active food packaging," *J. Food Eng.* 109(3), 520-524. DOI: 10.1016/j.jfoodeng.2011.10.030

Fatah, I., Abdul Khalil, H., Hossain, M., Aziz, A., Davoudpour, Y., Dungani, R., and Bhat, A. (2014). "Exploration of a chemo-mechanical technique for the isolation of nanofibrillated cellulosic fiber from oil palm empty fruit bunch as a reinforcing agent in composites materials," *Polymers* 6(10), 2611-2624. DOI: 10.3390/polym6102611

Haafiz, M. M., Eichhorn, S., Hassan, A., and Jawaid, M. (2013). "Isolation and characterization of microcrystalline cellulose from oil palm biomass residue," *Carbohyd. Polym.* 93(2), 628-634. DOI: 10.1016/j.carbpol.2013.01.035

Han, G., Huan, S., Han, J., Zhang, Z., and Wu, Q. (2014). "Effect of acid hydrolysis conditions on the properties of cellulose nanoparticle-reinforced polymethylmethacrylate composites," *Materials* 7(1), 16-29. DOI: 10.3390/ma7010016

Jonoobi, M., Khazaeian, A., Tahir, P. M., Azry, S. S., and Oksman, K. (2011). "Characteristics of cellulose nanofibers isolated from rubberwood and empty fruit bunches of oil palm using chemo-mechanical process," *Cellulose* 18(4), 1085-1095. DOI: 10.1007/s10570-011-9546-7

Lani, N. S., Ngadi, N., Johari, A., and Jusoh, M. (2014). "Isolation, characterization, and application of nanocellulose from oil palm empty fruit bunch fiber as nanocomposites," *Journal of Nanomaterials* 2014, 1-9. DOI: 10.1155/2014/702538

Li, R., Fei, J., Cai, Y., Li, Y., Feng, J., and Yao, J. (2009). "Cellulose whiskers extracted from mulberry: A novel biomass production," *Carbohyd. Polym.* 76(1), 94-99. DOI: 10.1016/j.carbpol.2008.09.034

Liu, D., Zhong, T., Chang, P. R., Li, K., and Wu, Q. (2010). "Starch composites reinforced by bamboo cellulosic crystals," *Bioresource Technol.* 101(7), 2529-2536. DOI: 10.1016/j.biortech.2009.11.058

Majeed, K., Jawaid, M., Hassan, A., Bakar, A. A., Abdul Khalil, H. P. S., Salema, A. A., and Inuwa, I. (2013). "Potential materials for food packaging from nanoclay/natural fibres filled hybrid composites," *Mater. Design* 46, 391-410. DOI: 10.1016/j.matdes.2012.10.044

Mandal, A., and Chakrabarty, D. (2011). "Isolation of nanocellulose from waste sugarcane bagasse (SCB) and its characterization," *Carbohyd. Polym.* 86(3), 1291-1299. DOI: 10.1016/j.carbpol.2011.06.030

Ng, H.-M., Sin, L. T., Tee, T.-T., Bee, S.-T., Hui, D., Low, C.-Y., and Rahmat, A. (2015). "Extraction of cellulose nanocrystals from plant sources for application as

reinforcing agent in polymers," *Compos. Part B-Eng.* 75, 176-200. DOI: 10.1016/j.compositesb.2015.01.008

Nishiyama, Y., Langan, P., and Chanzy, H. (2002). "Crystal structure and hydrogen-bonding system in cellulose Iβ from synchrotron X-ray and neutron fiber diffraction," *Journal of the American Chemical Society* 124(31), 9074-9082. DOI: 10.1021/ja0257319

Oksman, K., Mathew, A. P., Bondeson, D., and Kvien, I. (2006). "Manufacturing process of cellulose whiskers/polylactic acid nanocomposites," *Compos. Sci. Technol.* 66(15), 2776-2784. DOI: 10.1016/j.compscitech.2006.03.002

Pandey, J. K., Nakagaito, A. N., and Takagi, H. (2013). "Fabrication and applications of cellulose nanoparticle-based polymer composites," *Polym. Eng. Sci.* 53(1), 1-8. DOI: 10.1002/pen.23242

Rahimi Kord Sofla, M., Brown, R. J., Tsuzuki, T., and Rainey, T. J. (2016). "A comparison of cellulose nanocrystals and cellulose nanofibres extracted from bagasse using acid and ball milling methods," *Advances in Natural Sciences: Nanoscience and Nanotechnology* 7(3). DOI: 10.1088/2043-6262/7/3/035004

Ramli, R., Norhafzan, J., Beg, M. D. H., and Yunus, R. M. (2015). "Microcrystalline cellulose (MCC) from oil palm empty fruit bunch (EFB) fiber *via* simultaneous ultrasonic and alkali treatment," *International Journal of Chemical, Nuclear, Materials and Metallurgical Engineering* 9(1), 8-11.

Rosa, S. M., Rehman, N., de Miranda, M. I. G., Nachtigall, S. M., and Bica, C. I. (2012). "Chlorine-free extraction of cellulose from rice husk and whisker isolation," *Carbohyd. Polym.* 87(2), 1131-1138. DOI: 10.1016/j.carbpol.2011.08.084

Rosnah, M. S., Ku Halim, K. H., and Wan Hasamudin, W. H. (2002). "The potential of oil palm lignocellulosic fibres for the cellulose derivatives production," *Proc. of the Research and Consultancy Seminar*, 140-145.

Segal, L., Creely, J. J., Martin, A. E., and Conrad, C. M. (1959). "An empirical method for estimating the degree of crystallinity of native cellulose using the X-Ray diffractometer," *Textile Research Journal* 29(10), 786-794. DOI: 10.1177/004051755902901003

Tang, L., Huang, B., Lu, Q., Wang, S., Ou, W., Lin, W., and Chen, X. (2013). "Ultrasonication-assisted manufacture of cellulose nanocrystals esterified with acetic acid," *Bioresource Technol.* 127, 100-105. DOI: 10.1016/j.biortech.2012.09.133

Teixeira, E. d. M., Pasquini, D., Curvelo, A. A., Corradini, E., Belgacem, M. N., and Dufresne, A. (2009). "Cassava bagasse cellulose nanofibrils reinforced thermoplastic cassava starch," *Carbohyd. Polym.* 78(3), 422-431. DOI: 10.1016/j.carbpol.2009.04.034

Wang, N., Ding, E., and Cheng, R. (2007). "Thermal degradation behaviors of spherical cellulose nanocrystals with sulfate groups," *Polymer* 48(12), 3486-3493. DOI: 10.1016/j.polymer.2007.03.062

Yang, J., and Ye, D. Y. (2012). "Liquid crystal of nanocellulose whiskers' grafted with acrylamide," *Chinese Chem. Lett.* 23(3), 367-370. DOI: 10.1016/j.cclet.2011.12.014

Zahrim, A. Y., Asis, T., Hashim, M. A., Al-Mizi, T. M. T. M. A., and Ravindra, P. (2015). "A review on the empty fruit bunch composting: Life cycle analysis and the effect of amendment(s)," in: *Advances in Bioprocess Technology*, P. Ravindra (ed.), Cham: Springer International Publishing, pp. 3-15.

Article submitted: April 12, 2017; Peer review completed: June 1, 2017; Revised version received: June 24, 2017; Further revisions: July 11, 2017; Accepted: July 22, 2017; Published: August 1, 2017.
DOI: 10.15376/biores.12.3.6773-6788